Supplementary Information

Focused ion beam milling of self-assembled magnetic superstructures: an approach to fabricate nanoporous materials with tunable porosity

Verner Håkonsen[a], *Gurvinder Singh*[b,c], *Jianying He*[a] and *Zhiliang Zhang**[a]

[a] NTNU Nanomechanical Lab, Department of Structural Engineering, Norwegian University of Science and Technology (NTNU), Trondheim 7491, Norway.

[b] Department of Materials Science and Engineering, Norwegian University of Science and Technology (NTNU), Trondheim 7491, Norway.

[c] School of Aerospace, Mechanical and Mechatronic Engineering, University of Sydney, Sydney, NSW 2008, Australia.

*E-mail: zhiliang.zhang@ntnu.no

Experimental

Synthesis of monodisperse cubic and spherical $CoFe_2O_4$ nanoparticles

$CoFe_2O_4$ nanocubes were prepared by thermal decomposition of iron-cobalt oleate in the presence of sodium oleate, according to a modified protocol reported in the literature.[1] First, cobalt-iron oleate was prepared by mixing of iron (III) chloride ($FeCl_3 \cdot 6H_2O$, Alfa Aesar, 98 %) (5.40 g; 20 mmol), cobalt (II) chloride ($CoCl_2 \cdot 6H_2O$, Alfa Aesar, 98 %) (1.30 g; 10 mmol) and sodium oleate (TCI, >97 %) (18.25 g; 60 mmol) in a 250 mL round-bottom flask containing deionized water (40 mL), hexane (90 mL) and ethanol (40 mL). The reaction mixture was vigorously stirred under nitrogen atmosphere for four hours at T = 70 °C. The dark red organic product was separated from water and washed three times with water to remove reaction byproducts. The product was dried in vacuum at room temperature to remove residual water content, hexane and ethanol, and thereafter transferred to glass vial. The cobalt-iron oleate product was stored in a fridge ($T \approx 4$ °C).

To synthesize ~10 nm $CoFe_2O_4$ nanocubes, prepared oleate (1.62 g) and sodium oleate (0.42 g) were added to a 100 mL round-bottom flask containing 25 mL octadecene (Sigma Aldrich). The reaction mixture was heated to 320 °C at the rate of 3 °C min^{-1} under argon atmosphere, and left at this temperature for 45 min before cooled down to 100 °C. The nanocubes were obtained after washing the reaction product three times with toluene and isopropanol, and stored in toluene at room temperature. The spherical $CoFe_2O_4$ nanoparticles (~10 nm) were prepared by similar protocol except replacement of the sodium oleate with oleic acid (Alfa Aesar, technical grade, 90 %) (600 µL; 1.90 mmol).

Self-assembly of $CoFe_2O_4$ nanoparticles at the liquid-air interface

A hexane solution of nanoparticles (v = 100 µL, concentration, c = 8.5 mg mL^{-1}) containing oleic acid (3.5 µL mL^{-1}) was added onto the surface of diethylene glycol (2.2 mL), inside a polyethylene well of diameter ≈ 2 cm and height ≈ 2 cm. The well was cover with a glass slide to prevent the rapid evaporation of hexane, and the whole was setup left undistributed until all the hexane had evaporated (up to ~2 h). The self-assembled magnetic superstructures were transferred to silicon substrate by lift-off, and the samples were dried in vacuum to remove residual traces of diethylene glycol. Samples were thereafter gently washed with ethanol three times to remove excess oleic acid surfactant.

Focused ion beam milling

Focused ion beam (FIB) milling was performed in a FEI Helios NanoLab 600 DualBeam FIB, at ambient room temperature. As acceleration voltages during milling were set to 2, 5, 10, 15, 20, 25 and 30 kV, the corresponding applied beam currents were set to 6.7, 1.5, 2.9, 3.1, 1.8, 2.3 and 2.8 nA, respectively. The ion beam angle of incidence was set to 0°.

Characterization

If not stated otherwise, scanning electron microscopy (SEM) images were captured in the FEI Helios NanoLab 600 instrument by employing the electron beam. All images were captured in secondary electron mode at 5 kV, with beam current corresponding 86 pA.

The SEM images shown in Figure 4b, S1a-c, S12 and S13 were captured in secondary electron mode in a Hitachi S-5500 S(T)EM in-lens system, with acceleration voltage and emission current set to be 30 kV and 20 µA, respectively. Energy dispersive X-ray (EDX) mapping was performed with a Bruker XFlash EDX Detector in the same instrument, using the same beam parameters.

Transmission electron micrographs were captured in JEOL 2100, operating at 200 kV.

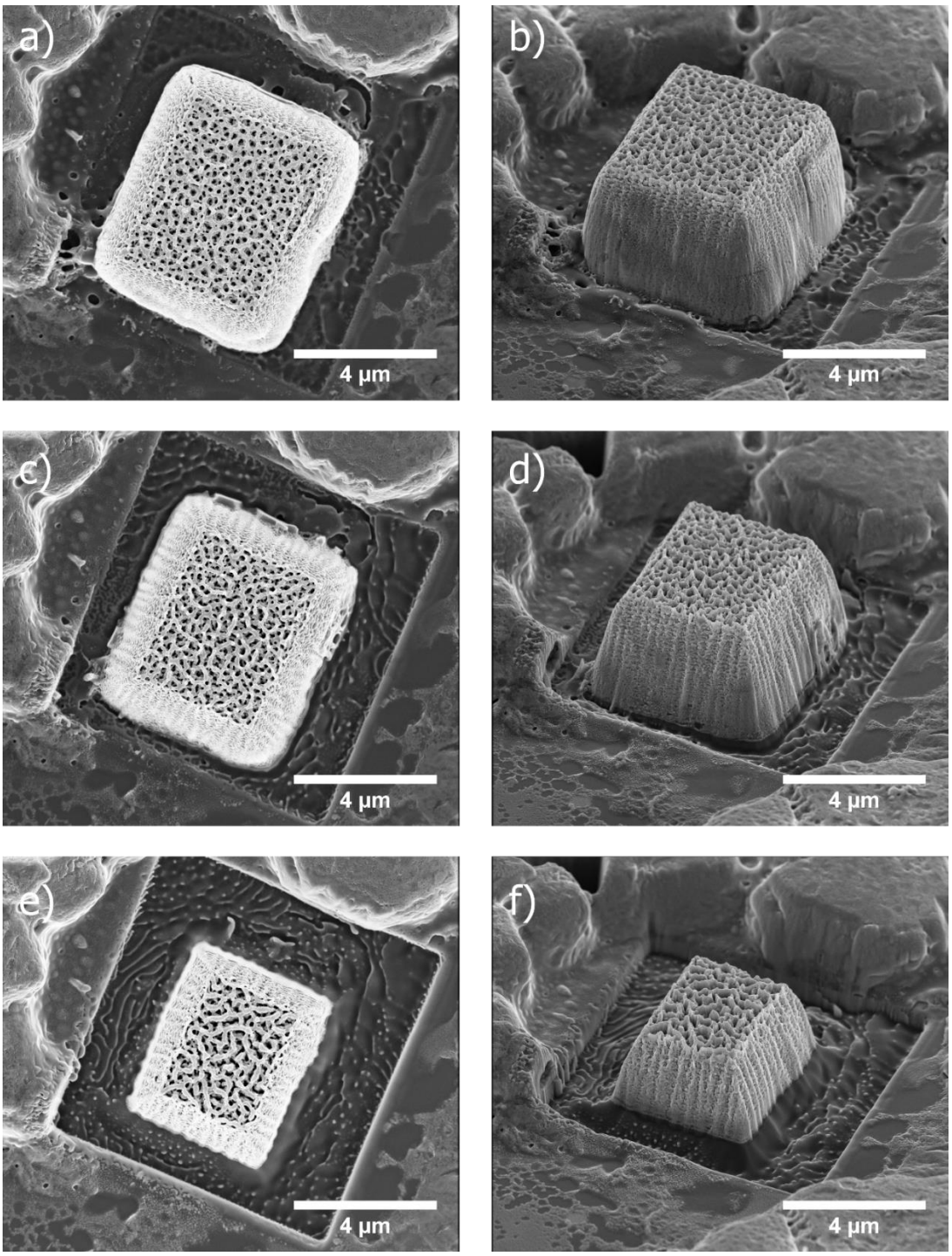

Fig. S1 SEM micrographs depicting pore structure evolution during ion beam milling of a cubic superstructure at 30 kV. a), c) and e) show top-view image of the supercube after exposure of a dose of 0.5, 1.0 and 2.0 nC μm^{-2}, respectively, while b), d) and f) show the same structure as the previous panel at a tilted angle of 52°. The pore size does not change drastically after extensive milling, but the superstructure shrinks as material is milled away. Since edges exhibit a higher milling rate, the supercube becomes more and more pyramidal as time progresses.

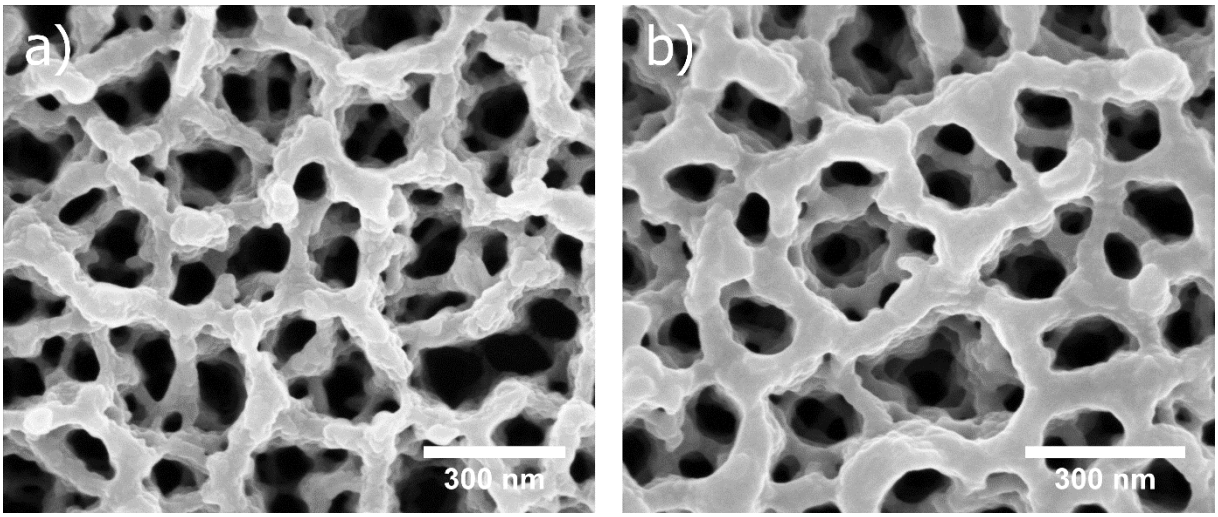

Fig. S2 Tuning the porosity of the resulting pore network after ion beam exposure of a nanosphere-based superstructure, by controlling the ion beam voltage at a constant dose of 0.5 nC μm^{-2}. a) and b) show SEM micrographs of the resulting pore network after ion beam exposure at 15 and 25 kV, respectively.

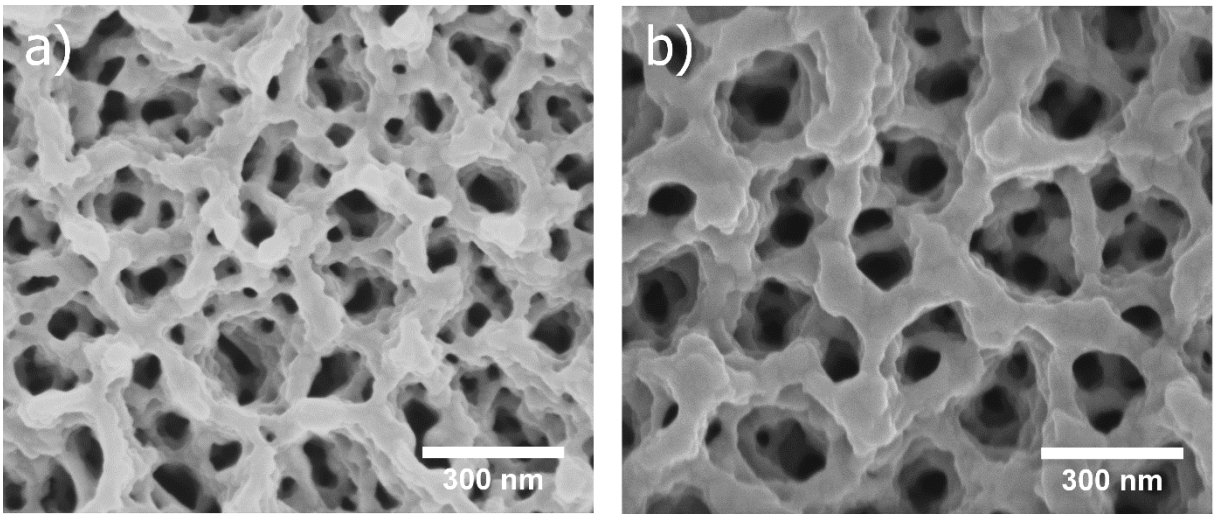

Fig. S3 Tuning the porosity of the resulting pore network after ion beam exposure of a nanocube-based superstructure, by controlling the ion beam voltage at a constant dose of 0.5 nC μm^{-2}. a) and b) show SEM micrographs of the resulting pore network after ion beam exposure at 15 and 25 kV, respectively.

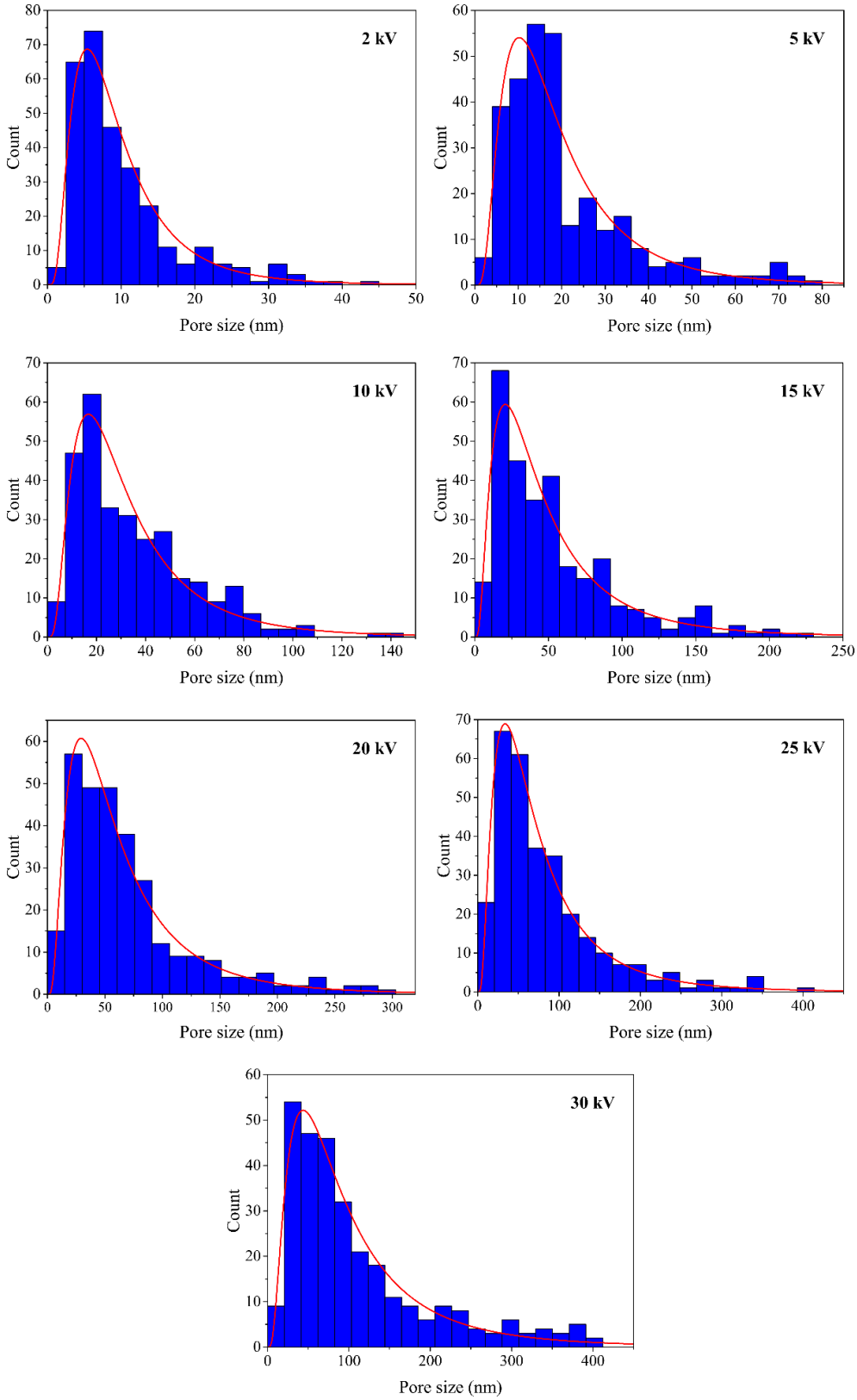

Fig. S4 Pore size distributions fitted with a lognormal distribution (red curves). Ion beam exposure at 2, 5, 10, 15, 20, 25 and 30 kV were considered for the nanosphere-based superstructure.

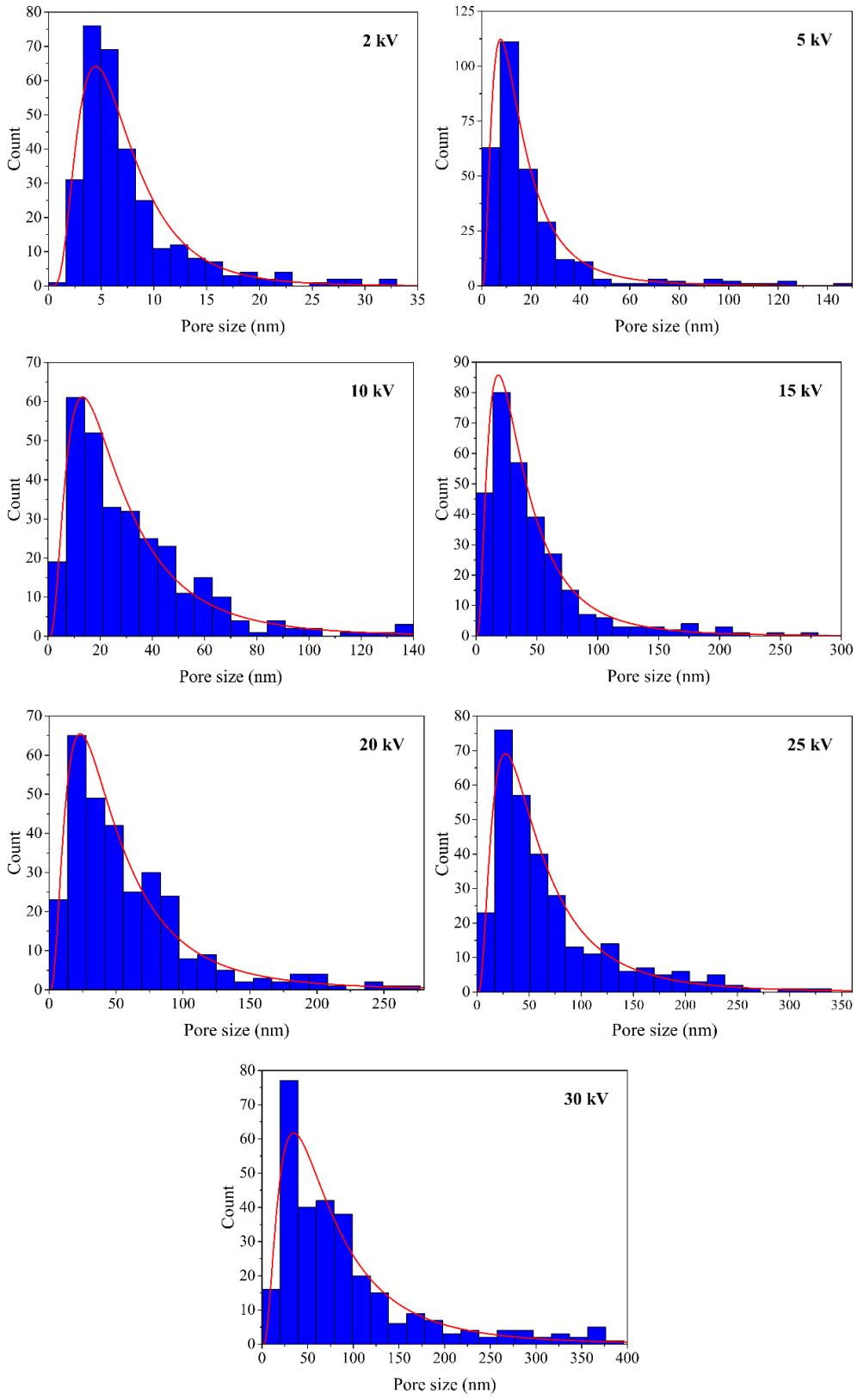

Fig. S5 Pore size distributions fitted with a lognormal distribution (red curves). Ion beam exposure at 2, 5, 10, 15, 20, 25 and 30 kV were considered for the nanocube-based superstructure.

Statistical analysis of pore size

After the sphere- and cube-based superstructures were exposed to the ion beam at acceleration voltages of 2, 5, 10, 15 20, 25 and 30 kV (maintaining a constant dose of 0.5 nC μm^{-2}), SEM images were captured at identical magnifications for easier comparison. The software *ImageJ* was used to set the accurate scale and measure the pores sizes of 300 pores for each case. Thereafter, the data was fitted to a lognormal distribution

$$p(x) = \frac{1}{x\sigma\sqrt{2\pi}} e^{-\frac{(\ln x - \mu)^2}{2\sigma^2}},$$

and the parameters μ and σ were extracted to calculate the mean, standard deviation and mode (*i.e.* the most probable pore size corresponding to the maximum of the probability distribution) according to $\exp(\mu + \frac{1}{2}\sigma^2)$, $\sqrt{[\exp(\sigma^2) - 1]\exp(2\mu + \sigma^2)}$ and $\exp(\mu - \sigma^2)$, respectively.[2] The extracted parameters, μ and σ, from the probability distributions are summarized in Table S1, for pore sizes resulting from all considered ion beam voltages.

The mean pore size was in general found to be linear with respect to the ion beam voltage (see main article), and the same holds true for the mode and the standard deviation, shown in Fig. S6. Linear curve fitting, *i.e.* to $y = ax + b$, was performed in the case of mean and mode, for both spheres and cubes, where the results are reported in Table S2. As observed from Fig. S7, the pore sizes are generally larger in the case of spheres compared to cubes, also reflected by the higher value of the *a*-parameter for spheres in Table S2. Interestingly, by extrapolating to zero ion beam voltage, the *b*-parameter is close the spacing between nanoparticles in the superstructure, *i.e.* ~2-3 nm, indicating there exists an intrinsic porosity of the unexposed superstructure (this holds true of the surfactant matrix is disregarded).

Table S1 Extracted parameters μ and σ from lognormal distributions, after fitting measured pore size data from sphere- and cube-based superstructures exposed at ion beam voltages 2, 5, 10, 15, 20, 25 and 30 kV. The parameters μ and σ can further be used to calculated the mean, standard deviation and mode of the distributions.

Voltage	μ_{sphere}	σ_{sphere}	μ_{cube}	σ_{cube}
2 kV	2.111	0.652	1.836	0.581
5 kV	2.793	0.686	2.635	0.775
10 kV	3.319	0.710	3.176	0.769
15 kV	3.682	0.809	3.526	0.785
20 kV	3.958	0.763	3.778	0.795
25 kV	4.131	0.786	3.930	0.791
30 kV	4.404	0.791	4.190	0.801

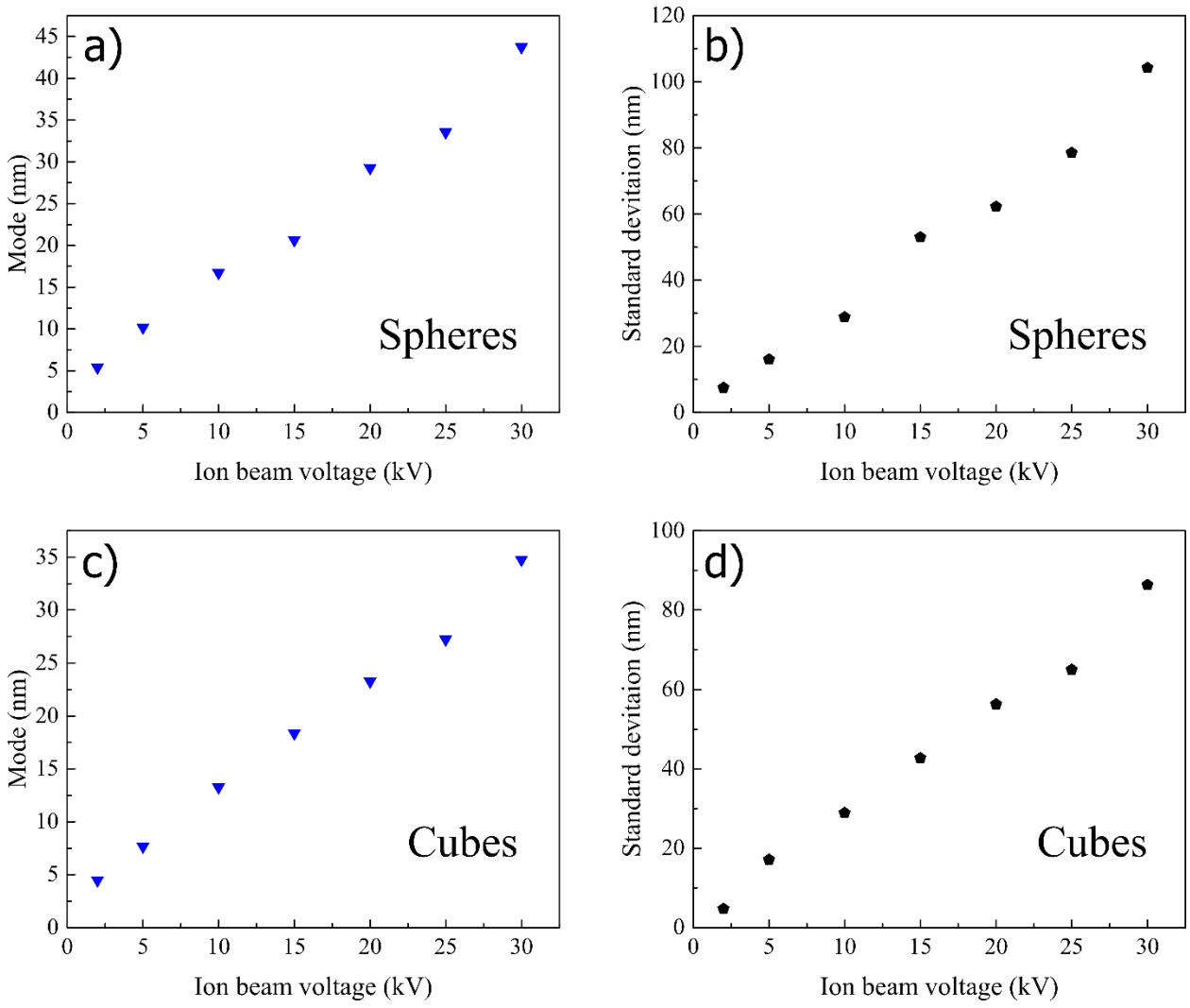

Fig. S6 Plotted mode and standard deviation of pore size as a function of ion beam voltage for spheres in a) and b), and cubes in c) and d). In all cases, a linear relationship is observed.

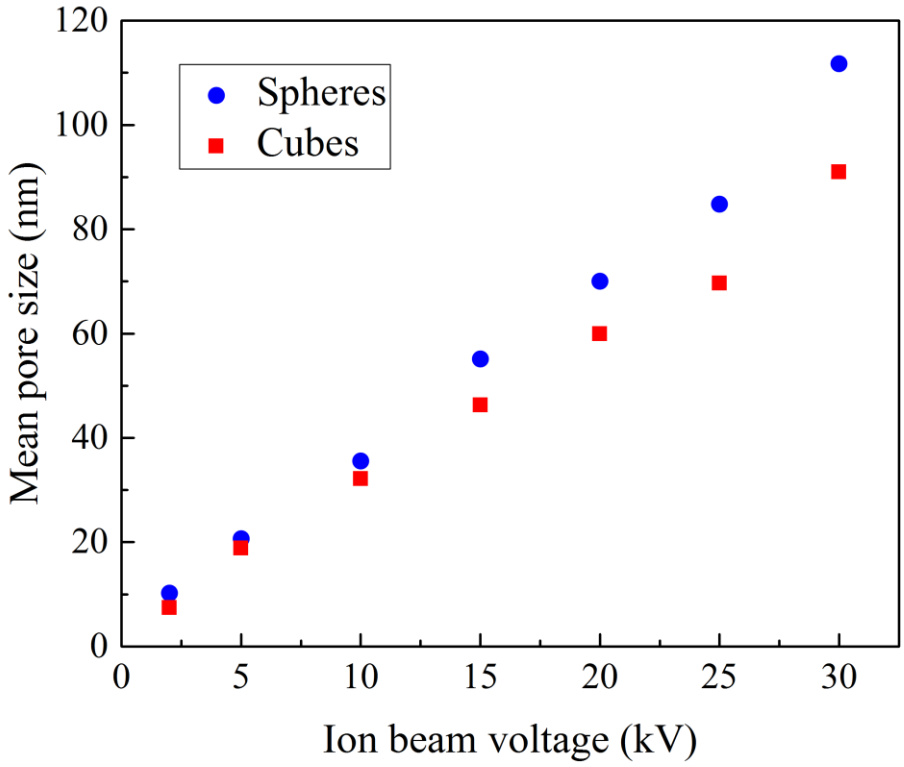

Fig. S7 Plotted mean pores size as a function of ion beam voltage, for both sphere- and cube-based superstructures.

Table S2. Extracted parameters a and b from the linear curve fitting ($y = ax + b$) of mean pore size and mode as a function of ion beam voltage, for both sphere- and cube-based superstructures.

Parameter	a [nm/kV]	b [nm]	R^2
Mean spheres	3.5	2.1	0.993
Mean cubes	2.8	3.2	0.994
Mode spheres	1.3	2.9	0.990
Mode cubes	1.0	2.5	0.996

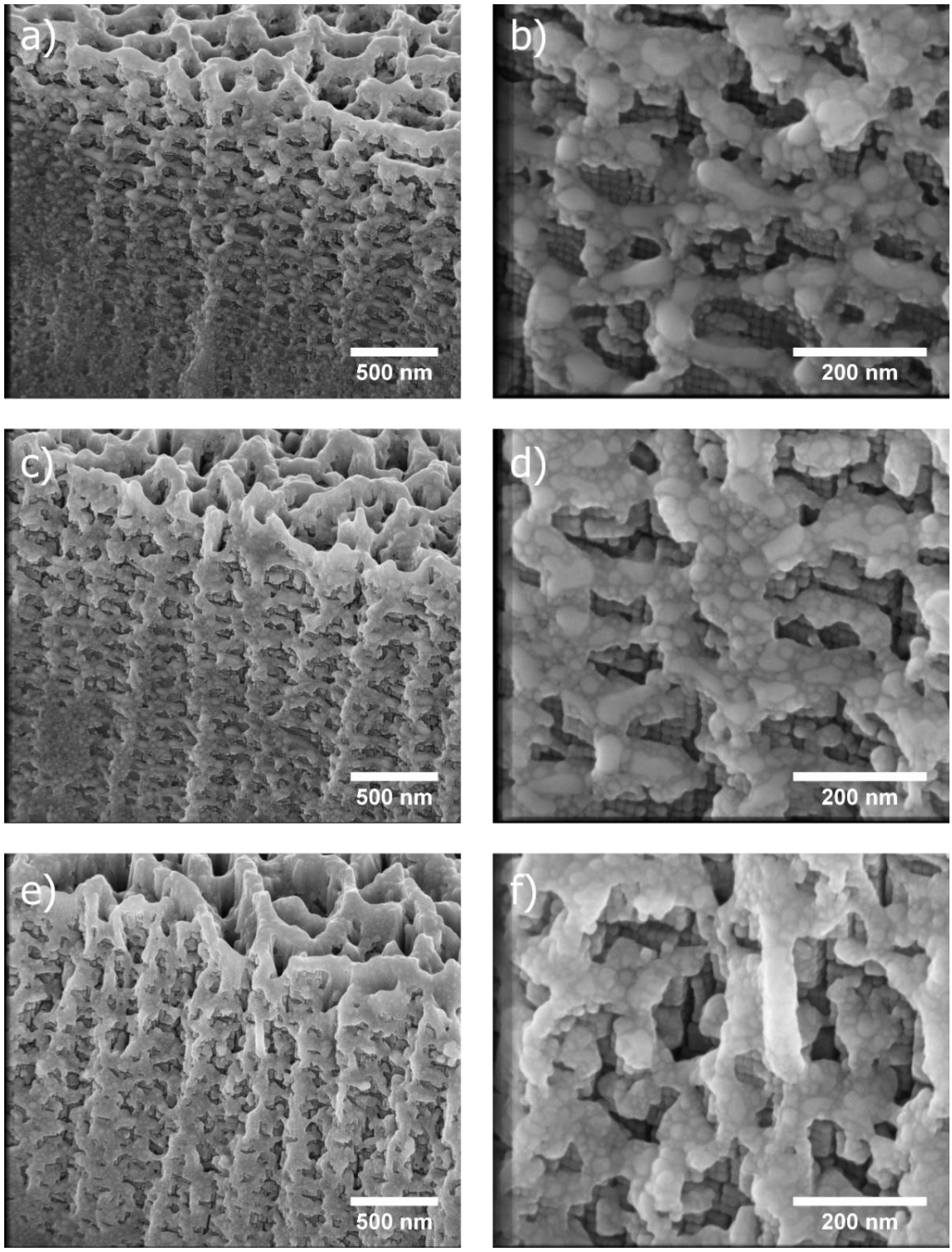

Fig. S8 SEM micrographs depicting pore structure evolution during FIB milling of a cubic superstructure at ion beam voltage 30 kV. The side of the superstructure is shown in all images, at a tilted angle of 52°. Images to the right show a close-up of the images to the left. a) and b) show the structure after exposure of an ion beam dose of 0.5 nC μm^{-2}. c) and d) show the structure after exposure of an ion beam dose of 1.0 nC μm^{-2}. e) and f) show the structure after exposure of an ion beam dose of 2.0 nC μm^{-2}. The stacking of nanocubes can be seen in the interior of the structure.

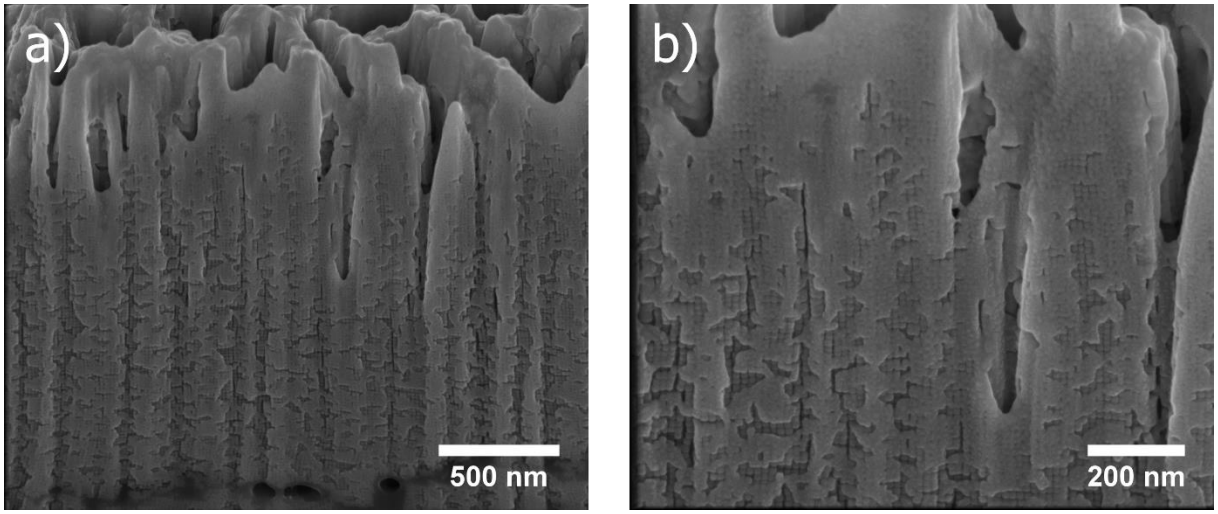

Fig. S9 SEM micrographs depicting a milled cross section of a cubic superstructure after being exposed to the ion beam at a voltage of 30 kV with dose 2.0 nC μm^{-2}. a) and b) show an overview and a close-up, respectively. After an exposure dose of 2.0 nC μm^{-2}, the porous backbone becomes thicker, and smaller networks disappear to a higher extent. Still, good coherent stacking of nanocubes remains existent within the interior of the structure. Melting of nanocubes can clearly be seen in the outermost parts of the porous network, which have been fully exposed to the ion beam.

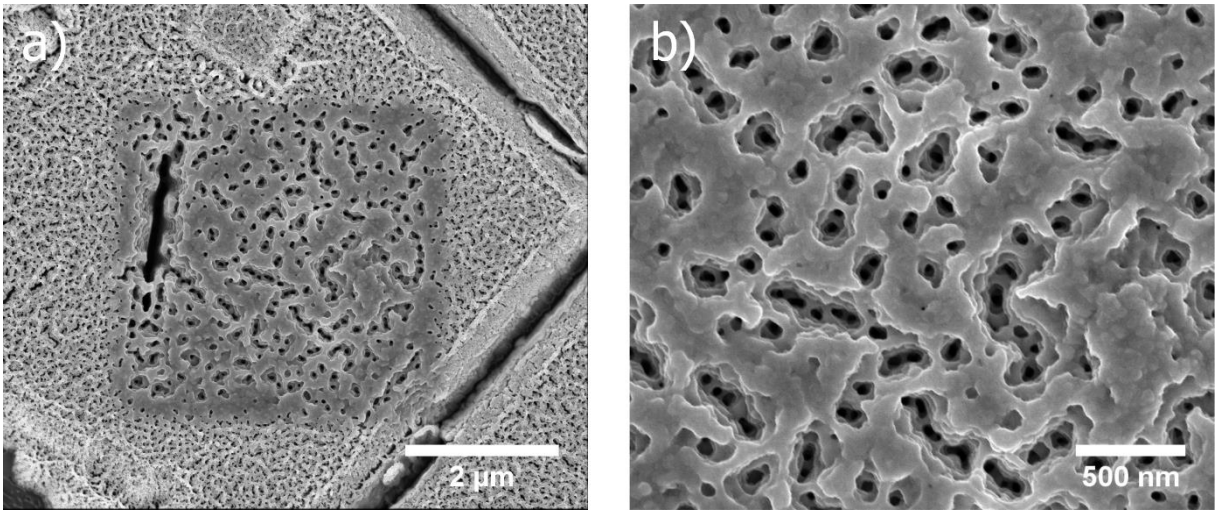

Fig. S10 Cubic superstructure exposed to FIB at acceleration voltage 5 kV with a dose corresponding to 0.5 nC μm^{-2}, then subsequently exposed again at 30 kV with a 0.1 nC μm^{-2} dose. a) and b) show an overview and a close-up SEM micrograph, respectively, of the part exposed at 30 kV. Larger pore backbones seems to grow at the expense of smaller ones, possibly due to a combination of melting and redeposition of material during milling, similar to an Ostwald ripening process.

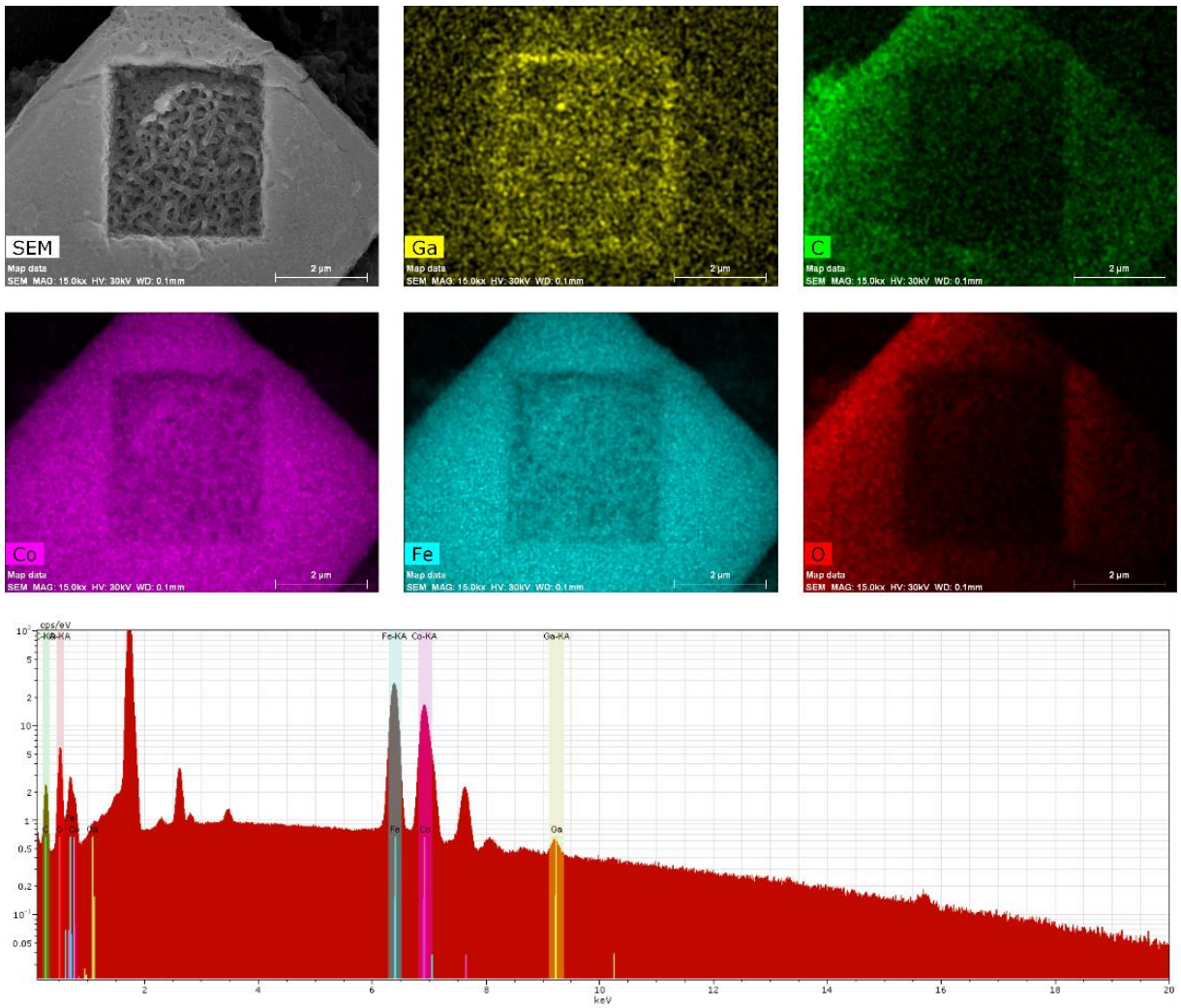

Fig. S11 EDX mapping of elements (Ga, C, Co, Fe and O) in a supercube, in which only a rectangular section of the surface has been exposed to the ion beam at 30 kV. Ga can clearly be observed in the area of exposure, as well as a peak in the spectrum, indicating implantation and presumably rendering the magnetism of the structure. It is also worth noting that the C-signal is significantly reduced in the exposed region, suggesting that any oleic acid surfactant readily vaporize during exposure.

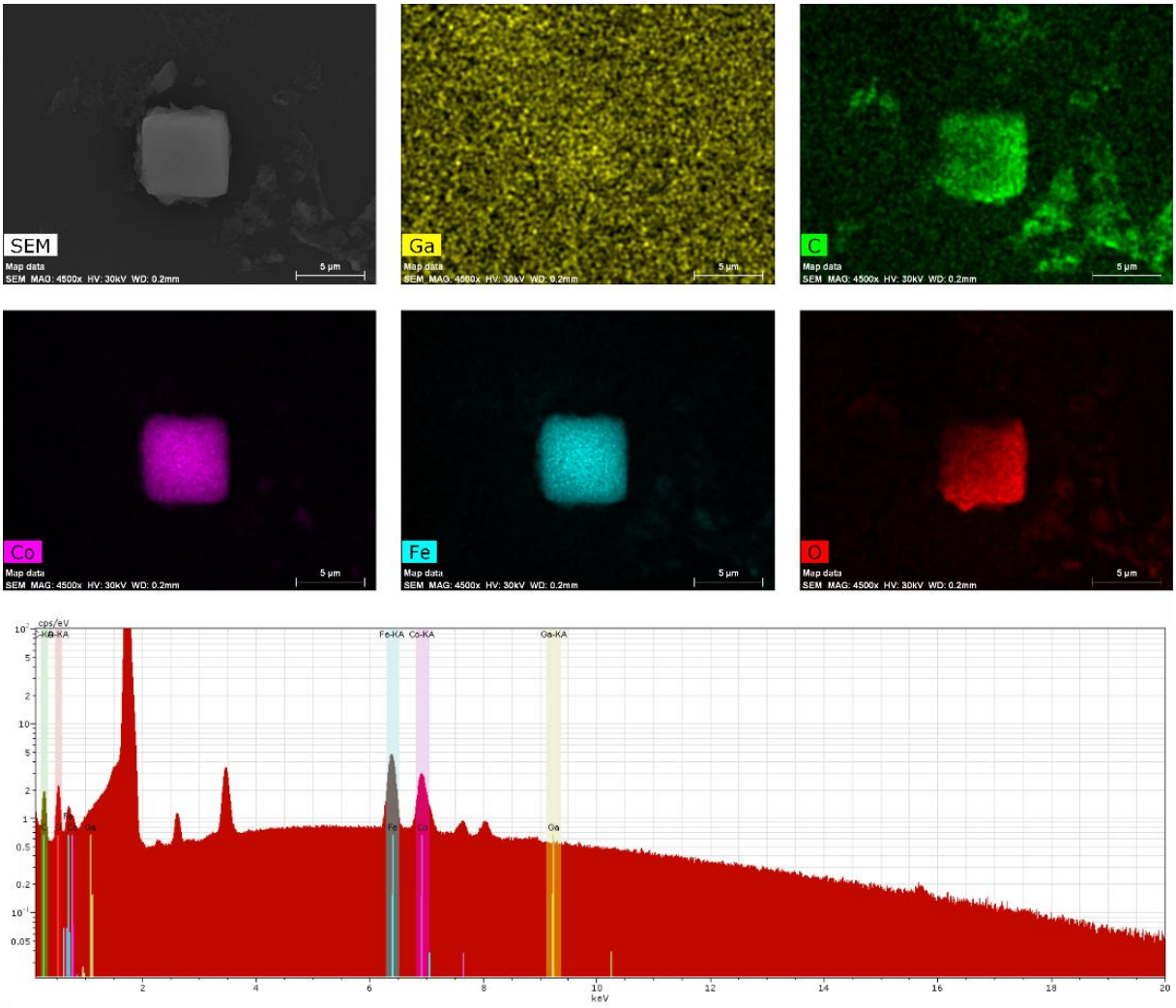

Fig. S12 EDX mapping of elements (Ga, C, Co, Fe and O) in an unexposed supercube. Only background signal is detected for Ga, and there is no corresponding peak in the spectrum. Evidently, Ga is in this case confirmed to be absent in the unexposed structure.

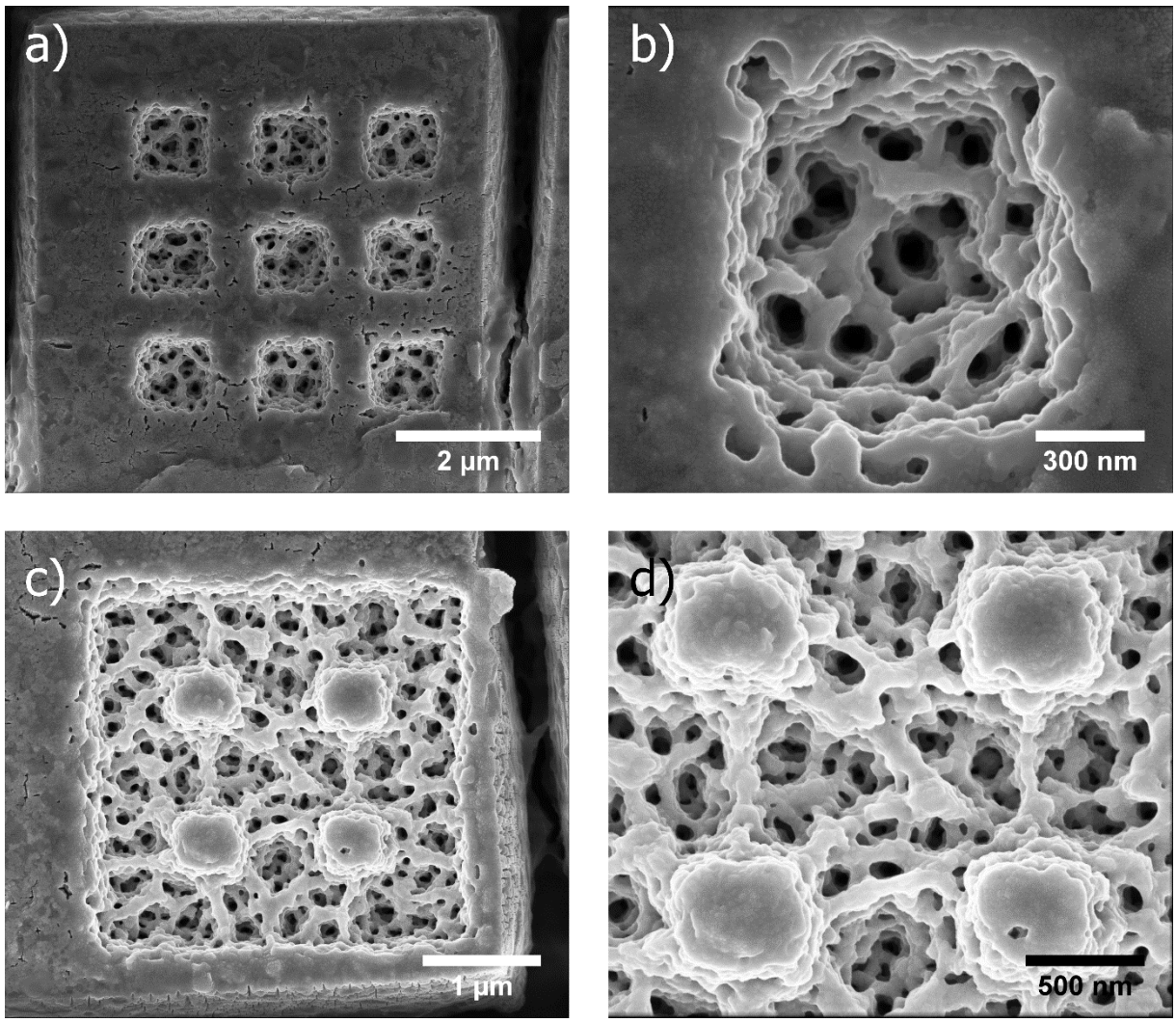

Fig. S13 FIB enables local patterns to be milled in individual superstructures. a) and b) show an overview and a close-up SEM micrograph, respectively, of a 3×3 array of milled squares. c) and d) show an overview and a close-up SEM micrograph, respectively, of an inverted pattern with respect to a) and b), where 2×2 pillars are surrounded by porous structure. Both patterns were milled at an ion beam acceleration voltage of 30 kV with a 0.5 nC μm^{-2} dose.

References

1 N. Bao, L. Shen, P. Padhan and A. Gupta, *Appl. Phys. Lett.*, 2008, **92**, 173101.

2 N. L. Johnson, S. Kotz and N. Balakrishnan, in *Continuous Univariate Distributions*, Vol. 1, John Wiley & Sons, New York, 2nd ed., 1994, Ch. 14.